Electronic Supplementary Material (ESI) for Reaction Chemistry & Engineering.

Supporting Information

for:

Unravelling the redox mechanism and kinetics of a highly active and selective Ni-based material during the oxidative dehydrogenation of ethane

Carlos Alvarado-Camacho,[a,b] Jeroen Poissonnier, [b] Joris W. Thybaut,[b] and Carlos O. Castillo[a*]*

[a]Laboratory of Catalytic Reactor Engineering applied to Chemical and Biological Systems. Departamento de Ingeniería de Procesos e Hidráulica. Universidad Autónoma Metropolitana-Iztapalapa, Av. San Rafael Atlixco 186, Col. Vicentina C.P. 09340, Ciudad de México, México

[b]Laboratory for Chemical Technology, Ghent University, Technologie park 125, B-9052 Ghent, Belgium.

Supplementary §1 Characterization techniques.

This section describes the equipment and the methodology followed to carry out the characterization of the SnO_2-NiO catalyst, including physisorption of N_2, XRD, XPS, O_2-TPEI, NH_3-TPD, H_2-TPR, and SEM-EDX. In addition, a table that summarizes the information extracted from each characterization technique is presented at the end of the §1.

N_2 physisorption was carried out by using a Micromeritics Tristar II 3020 equipment, The powder was preconditioned the powder at 573 K for 3 h to eliminate physically adsorbed components such as CO_2 and H_2O. The specific surface area was calculated by the Brunauer-Emmett-Teller (BET) method applying the classical five-point method ($0.05 < p/p0 < 0.35$) in a relative pressure range from 0.01 to 0.99, while the pore size distribution was determined by the Barret-Joyner-Hallender (BJH) method.

Surface morphologies were imaged by field-emission scanning electron microscopy (FESEM) with a JEOL 7600 FESEM set at 5 kV. The technique was employed to examine the morphology and to obtain the particle size distribution of the sample. Post-processing of the images was performed using ImageJ ® software.

Powder X-ray diffraction (XRD) pattern was obtained by using a Siemens Diffractometer Kristalloflex D5000 equipped with a monochromatic Cu Kα (8.040 keV, λ = 0.15418 nm) as the radiation source. Powder diffraction patterns were collected between $2\theta = 10°$ and $2\theta = 80°$, applying a step of 0.02° and 30s counting time for each angle. The mean crystallite diameter of the sample was calculated using the Scherrer's equation.

X-ray photoelectron spectroscopy (XPS) analysis was conducted using an S-Probe XPS spectrometer (VG, Surface Science Instruments), equipped with a monochromatized 450W Al Kα radiation source ($h\nu$ = 1486.6 eV). The base pressure of the analysis chamber was below $2x10^{-7}$ Pa. Spectra were recorded with 200W source power. The analyzer axis formed an angle of 45° with the specimen surface. Wide scan spectra were measured with a pass energy of 141 eV and a 0.22 eV step, while core levels were recorded with a step of 0.1

eV and a pass energy of 90.3 eV. C1s at 284.6 eV was used for alignment. Post-processing of the XPS spectrum was completed with the CasaXPS software.

Temperature-Programmed Isotope Exchange (TPIE) was carried out in a Micromeritics AutoChem II 2920 setup. The sample was pretreated in 10% $^{16}O_2$/He (140 cm3/min) at 450ºC during ca. 30 minutes in order to remove adsorbates and obtain the sample totally oxidized. After cooling down in Helium to 100ºC in order to remove adsorbed oxygen, a temperature-programmed isotope exchange experiment was performed by applying a linear temperature ramp (15ºC/min) under a 7/1% $^{18}O_2$/He flow (140 cm^3/min) until it reached 670ºC. The pressure was always near-ambient. The product gas composition was monitored by means of a thermal conductivity detector (TCD) and an online OmniStar (Pfeiffer Vacuum) mass spectrometer.

H_2 temperature programmed reduction (H_2-TPR) analysis was performed using a Micromeritics Autochem II 2920 chemisorption analyzer. In this experiment, the sample was pretreated with Argon (50 cm^3/min) at 450ºC for 60 minutes to remove the presence of adsorbates. After cooling down the sample to 40ºC in an inert atmosphere, the H_2-TPR experiment initiated by increasing the temperature following a linear ramp (10ºC/min) under an H_2/Ar flow (50 cm^3/min) until it reached 800ºC. The product gas composition was monitored using a thermal conductivity detector (TCD).

Temperature-programmed desorption of ammonia (NH_3-TPD) was performed in a Micromeritics AutoChem II 2920 equipment. The sample was pretreated with helium (50 cm^3/min) at 450ºC for 30 minutes to remove adsorbates. A flowrate of 4% NH_3-He at 75 cm^3/min for two hours was used to saturate the surface sample with ammonia. Then, helium was flowed at 60 cm^3/min for 30 minutes to desorb NH_3. TPD pattern was obtained by applying a linear temperature ramp (10ºC/min) under a helium flowrate of 60 cm^3/min until the temperature reached 700ºC. The desorption of NH_3 was monitored with a thermal conductivity detector (TCD) and an online OmniStar (Pfeiffer Vacuum) MS.

Table S1 . Summary of the information obtained from the characterization of the catalyst.

Characterization Technique	**Type of information obtained from the NiSnO catalyst**
N_2 Physisorption	BET surface area and pore size distribution.
Field-Emission Scanning Electron Microscopy (FESEM-EDX)	Morphological characteristics of the surface and particle size distribution. Local composition and the elemental atomic distribution.
X-Ray Diffraction (XRD)	Identification of crystalline structures and estimation of the average crystallite size.
X-ray photoelectron spectroscopy (XPS)	Quantitative determination of the atomic contents and signs about the oxidation state and chemical environment of the elements.
Temperature-Programmed $^{18}O_2$ Isotope Exchange (TPIE-$^{18}O_2$)	Mobility and exchangeability of the oxygen species from the catalyst lattice. Interaction between different oxygen species, in the lattice, surface and gas phase.
H_2 Temperature Programmed Reduction (H_2-TPR)	Reduction behaviour of the surface.
Temperature-programmed desorption of ammonia (NH_3-TPD)	Acid character of the catalytic sites.

Supplementary §2 External transport limitation, isothermal reactor response, homogeneous ODH-C_2 test and effect of the Ni/Sn atomic ratio.

This section presents figures obtained by an experimental evaluation focusing on external transport limitations (Figure S1a), the transient temperature response (Figure S1b) at two different axial positions in the micro-reaction unit as proof of the isothermal mode operation and homogeneous ODH-C_2 (Figure S1c) tests at different operating conditions.

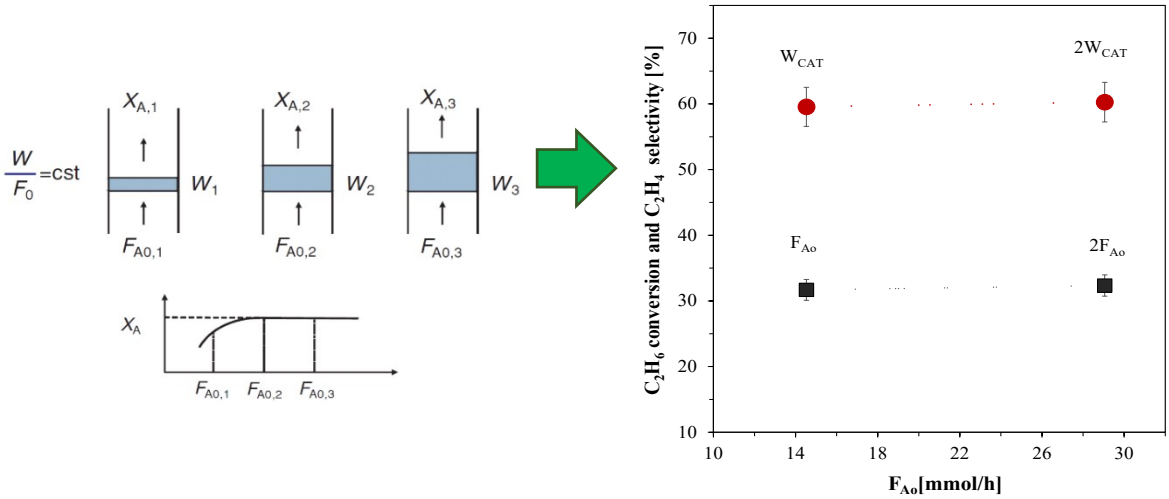

Figure S1a Effect of the total feed flow rate on the observed kinetics.

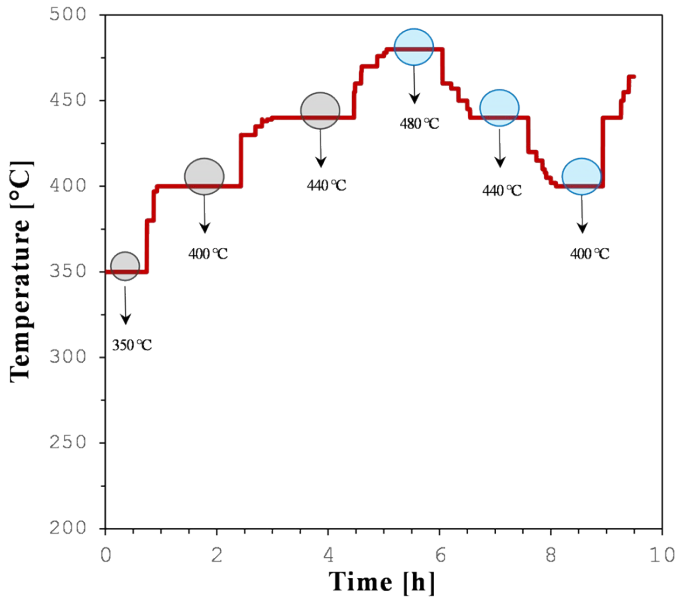

Figure S1b Isothermal mode operation in the micro-reaction unit.

The ODH-C_2 catalytic experiments were performed at a constant GHSV of 210 h^{-1}. Herein, the GHSV for ODH-C_2-homogeneous experiments is calculated based on the total volume of the reactor (i.e., a stainless-steel tubular fixed bed reactor with an internal diameter of 9 mm and a length of 305 mm). Based on Figure S1c, we can safely assume that no homogeneous reactions will occur in the range where the catalytic experiments were performed, i.e., at temperatures from 360 to 480 °C and a total pressure of 1 bar. Therefore, based on the temperature difference, tests with silicon carbide only for the homogeneous ODH-C_2 has no repercussions in this study since the homogeneous reaction would occur only if the activation energy can be overcome, being independent of of the residence time.

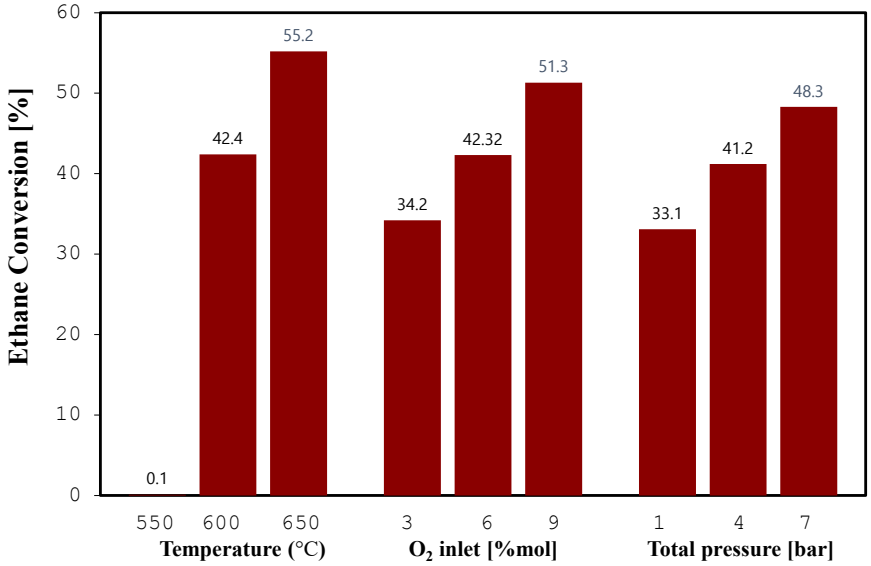

Figure S1c Homogeneous oxidative dehydrogenation of ethane, effect of temperature $\%O_2$ in the feed and total pressure on the ethane conversion. Conditions, temperature: P_T=1 bar,$\%O_{2in}$=6, $\%C_2H_{6in}$=9, O_2 inlet: P_T=1 bar, $\%C_2H_{6in}$=9, T=600°C, and total pressure: T=600°C, $\%C_2H_{6in}$=9, $\%O_{2in}$=3.

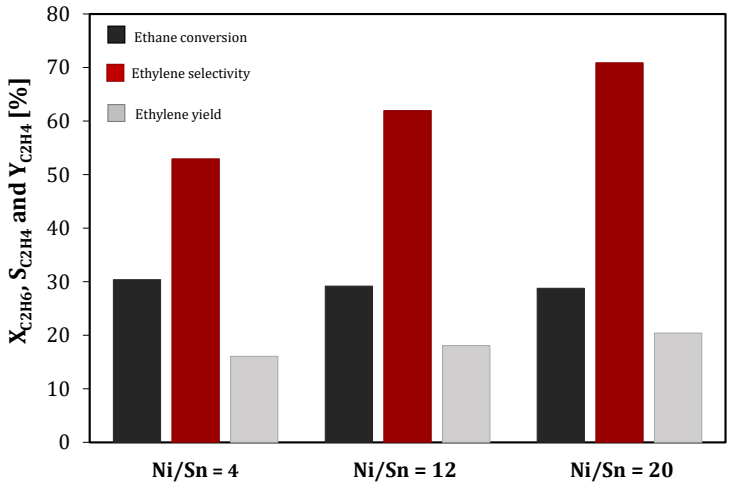

Figure S1d Oxidative dehydrogenation of ethane on NiO-SnO_2 material. Effect of the Ni/Sn atomic ratio. Conditions: PT=1 bar,%O2in=3, %C_2H_6in=9, T=450°C.

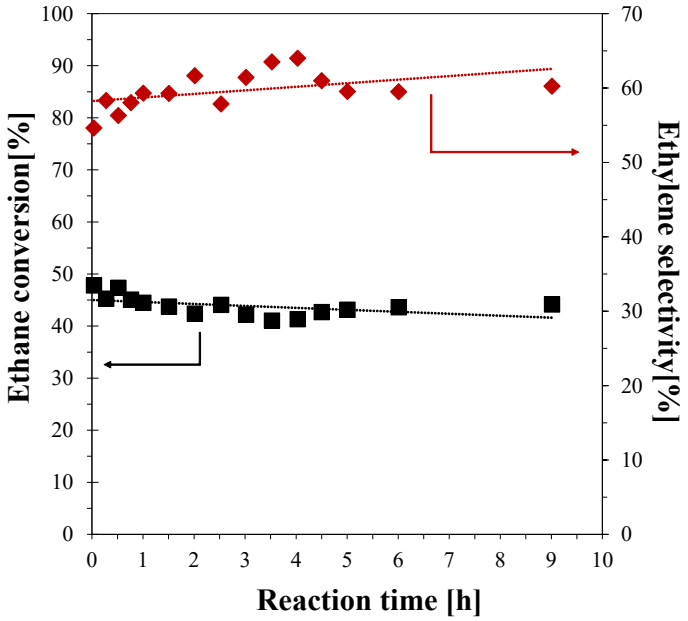

Figure S1e Evolution of the conversion of ethane and selectivity to ethylene with the time on line. Reaction conditions: T = 480 °C; W/F_{A0} = 45.54 kg_{cat} s $mol^{-1}{}_{C2H6}$; $C_2/O_2/N_2$ = 7/6/87

Supplementary §3 Reaction rates for LHHW, ER and MvK model

This section presents the equations for the LHHW, ER and MvK models following the pseudo-steady-state approach.

LHHW MODEL

The surface adsorption, desorption and reaction rates are given as follows:

Oxygen adsorption: $r_A^f = k_A^f N_T p_{O_2} \theta_S^2 \ , \ r_A^r = k_A^r N_T \theta_O^2$ * MERGEFORMAT (1)

Ethane adsorption: $r_B^f = k_B^f N_T p_{C_2H_6} \theta_S \ , \ r_B^r = k_B^r N_T \theta_{C_2H_6}$ * MERGEFORMAT (2)

Reaction 1: $r_1 = k_1 N_T \theta_{C_2H_6} \theta_O$ * MERGEFORMAT (3)

Reaction 2: $r_2 = k_2 N_T \theta_{C_2H_6} \theta_O$ * MERGEFORMAT (4)

Reaction 3: $r_3 = k_3 N_T \theta_{C_2H_4} \theta_O$ * MERGEFORMAT (5)

Ethylene adsorption: $r_C^f = k_C^f N_T \theta_{C_2H_4} \ , \ r_C^r = k_C^r N_T p_{C_2H_4} \theta_S$ * MERGEFORMAT (6)

CO_2 adsorption: $r_D^f = k_D^f N_T \theta_{CO_2} \ , \ r_D^r = k_D^r N_T p_{CO_2} \theta_S$ * MERGEFORMAT (7)

H_2O adsorption: $r_E^f = k_E^f N_T \theta_{H_2O} \ , \ r_E^r = k_E^r N_T p_{H_2O} \theta_S$ * MERGEFORMAT (8)

The concentration of the intermediate species, i.e., adsorbed species, are given as follows:

$$N_T \frac{d\theta_O}{dt} = 2\left(r_A^f - r_A^r\right) - r_1 - 7r_2 - 6r_3 = 0 \quad \text{* MERGEFORMAT (9)}$$

$$N_T \frac{d\theta_{C_2H_6}}{dt} = \left(r_B^f - r_B^r\right) - r_1 - r_2 = 0 \quad \text{* MERGEFORMAT (10)}$$

$$N_T \frac{d\theta_{C_2H_4}}{dt} = r_1 - r_3 - \left(r_C^f - r_C^r\right) = 0 \qquad \text{* MERGEFORMAT (11)}$$

$$N_T \frac{d\theta_{CO_2}}{dt} = 2r_2 + 2r_3 - \left(r_D^f - r_D^r\right) = 0 \qquad \text{* MERGEFORMAT (12)}$$

$$N_T \frac{d\theta_{H_2O}}{dt} = r_1 + 3r_2 + 2r_3 - \left(r_E^f - r_E^r\right) = 0 \qquad \text{* MERGEFORMAT (13)}$$

The global balance of the fraction sites corresponds to:

$$\theta_S + \theta_O + \theta_{C_2H_6} + \theta_{C_2H_4} + \theta_{CO_2} + \theta_{H_2O} = 1 \qquad \text{* MERGEFORMAT (14)}$$

ER MODEL

The surface adsorption, desorption and reaction rates can be expressed as follows:

Oxygen adsorption: $r_A^f = k_A^f N_T p_{O_2} \theta_S^2$, $r_A^r = k_A^r N_T \theta_O^2$ * MERGEFORMAT (15)

Reaction 1: $r_1 = k_1 N_T P_{C_2H_6} \theta_O$ * MERGEFORMAT (16)

Reaction 2: $r_2 = k_2 N_T P_{C_2H_6} \theta_O$ * MERGEFORMAT (17)

Reaction 3: $r_3 = k_3 N_T P_{C_2H_4} \theta_O$ * MERGEFORMAT (18)

H_2O adsorption: $r_E^f = k_E^f N_T \theta_{H_2O}$, $r_E^r = k_E^r N_T p_{H_2O} \theta_S$ * MERGEFORMAT (19)

The concentration of the intermediate species, i.e., the adsorbed oxygen and

the adsorbed water can be expressed as:

$$N_T \frac{d\theta_O}{dt} = 2\left(r_A^f - r_A^r\right) - r_1 - 7r_2 - 6r_3 = 0 \qquad \text{* MERGEFORMAT (20)}$$

$$N_T \frac{d\theta_{H_2O}}{dt} = r_1 + 3r_2 + 2r_3 - \left(r_E^f - r_E^r\right) = 0 \qquad \text{* MERGEFORMAT (21)}$$

And the global balance of the fraction sites corresponds to:

$$\theta_S + \theta_O + \theta_{H_2O} = 1 \qquad \text{* MERGEFORMAT (22)}$$

MvK MODEL

The surface reaction rates, including the re-oxidation rate can be expressed according to the following equations:

Reaction 1: $r_1 = k_1 N_T P_{C_2H_6} \theta_{Ox}$ * MERGEFORMAT (23)

Reaction 2: $r_2 = k_2 N_T P_{C_2H_6} \theta_{Ox}$ * MERGEFORMAT (24)

Reaction 3: $r_3 = k_3 N_T P_{C_2H_4} \theta_{Ox}$ * MERGEFORMAT (25)

Re-oxidation rate: $r_O = k_O^f P_{O_2} N_T \theta_{\text{Red}}^2 - k_O^r \theta_{\text{Ox}}^2$ * MERGEFORMAT (26)

The concentration of oxidized sites in the surface is determined by:

$$N_T \frac{d\theta_{Ox}}{dt} = 2r_O - r_1 - 7r_2 - 6r_3 \qquad \text{* MERGEFORMAT (27)}$$

And the global balance of the fraction sites corresponds to:

$$\theta_{Ox} + \theta_{\mathrm{Red}} = 1 \qquad \text{* MERGEFORMAT (28)}$$

Supplementary §4 Figures obtained by the characterization techniques.

This section presents figures obtained by the characterization techniques described in Supplementary §1, such as XRD patterns, SEM micrographs, EDX elemental maps, XPS spectrum, and adsorption-desorption isotherms.

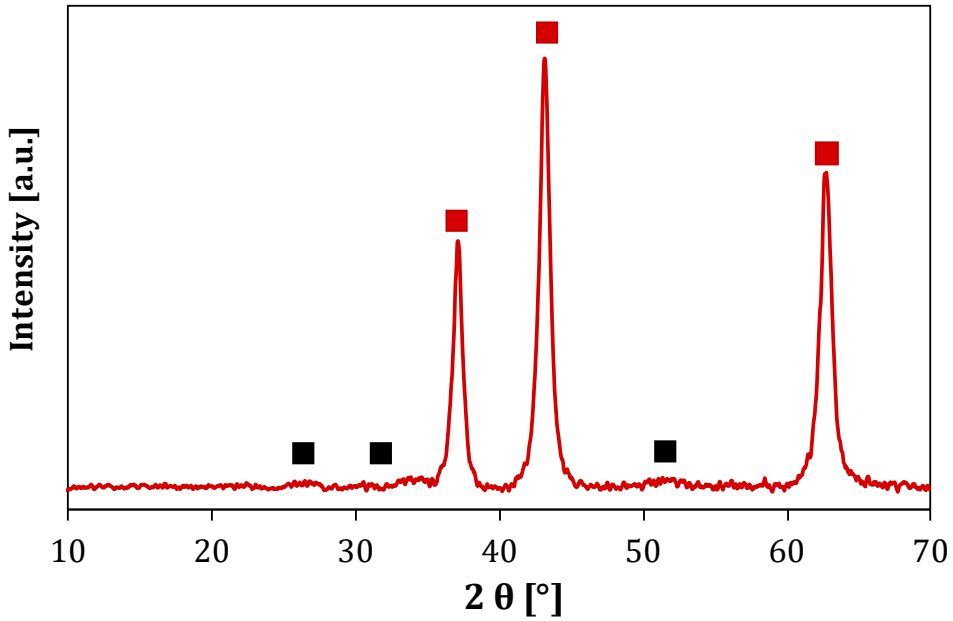

Figure S2 X-ray diffraction (XRD) patterns of Ni–Sn–O catalyst. Markups: ■ SnO_2 (JCPDS 41-1445); ■ NiO (JCPDS 78-0643).

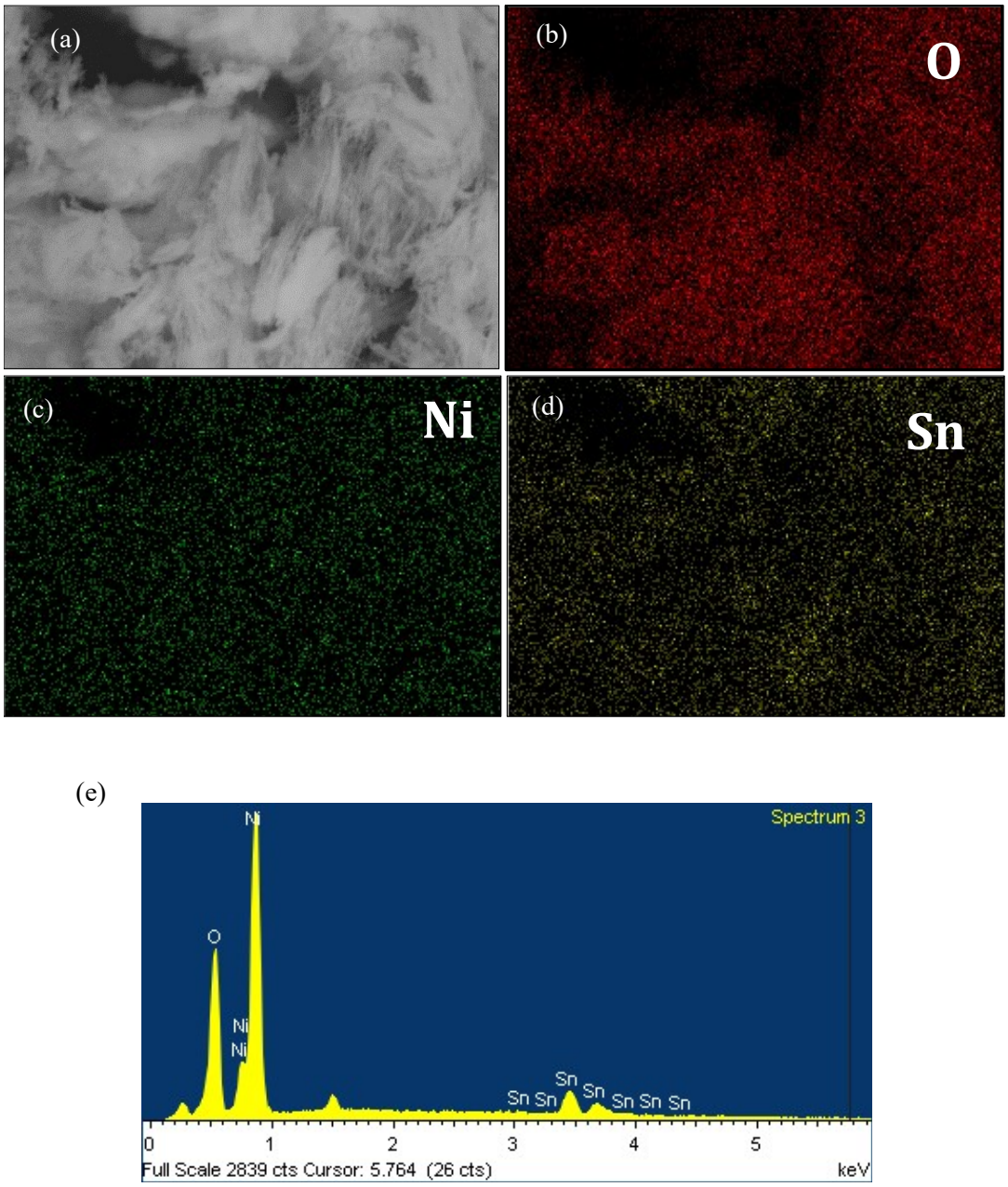

Figure S3 SEM micrographs and corresponding EDX elemental analysis of NiSnO catalyst, a) SEM micrograph, b) O Kα1, c) Ni Kα1, d) Sn Lα1 and e) elemental atomic compositions.

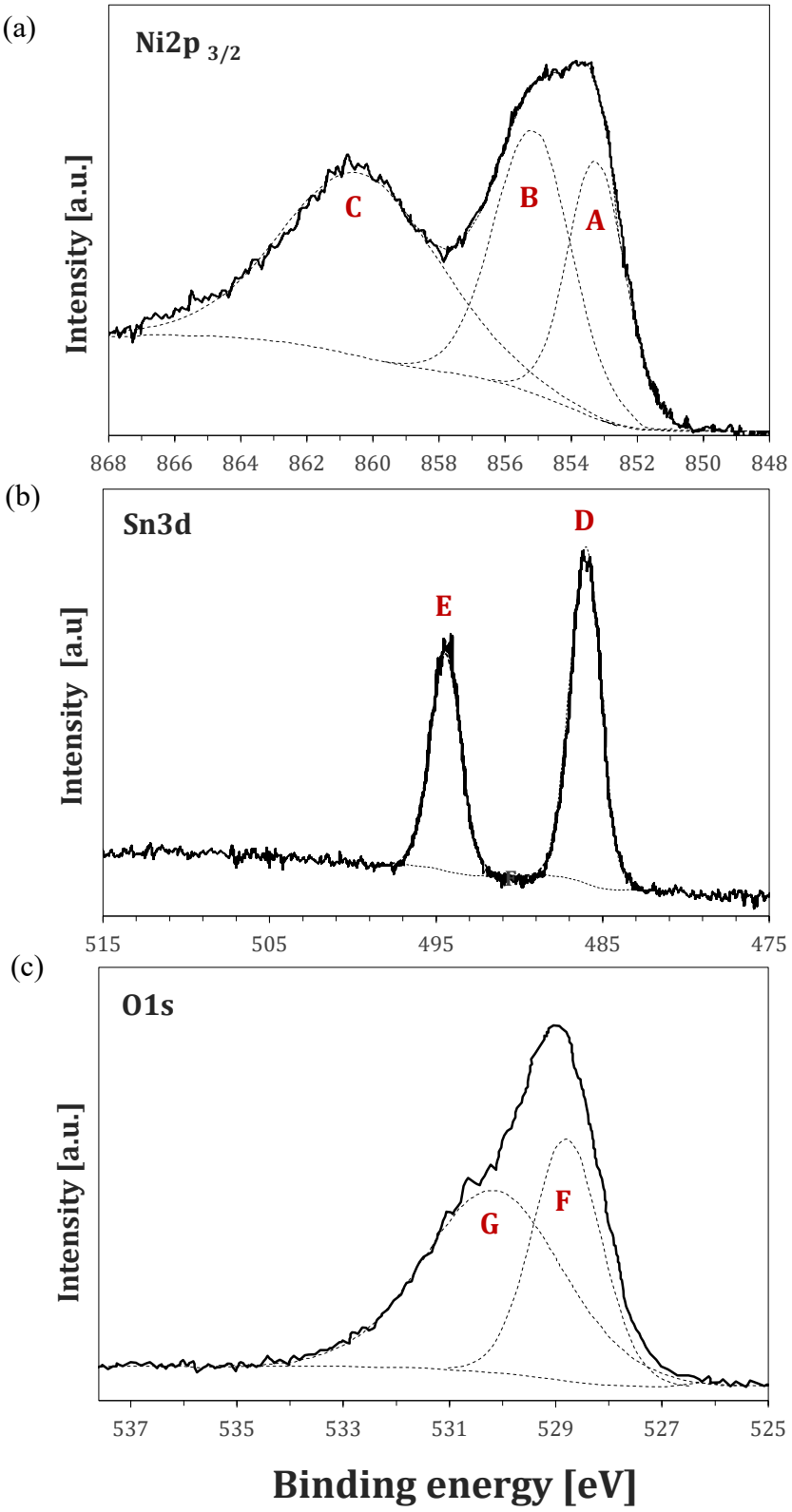

Figure S4 X-ray photoelectron spectroscopy (XPS) analysis for the SnO_2-NiO sample. a) Ni $2p_{3/2}$ core level state; b) Sn3d core level state ; and c) O1s core level state.

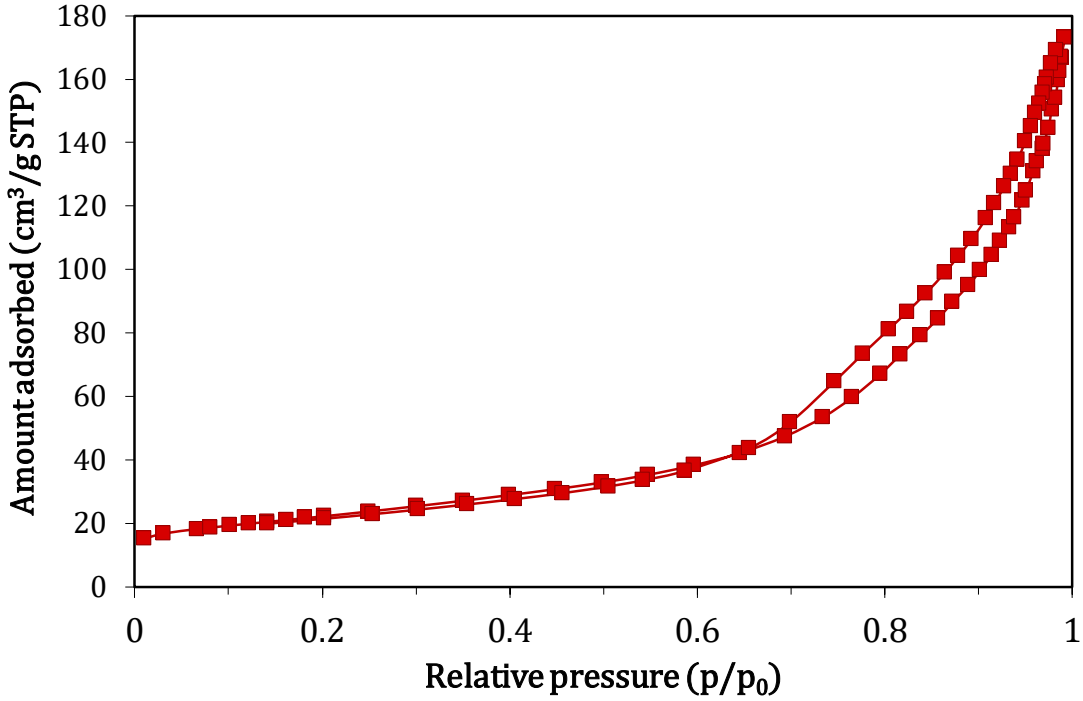

Figure S5 N_2 adsorption-desorption isotherm for the SnO_2-NiO catalyst, measured at 77K.

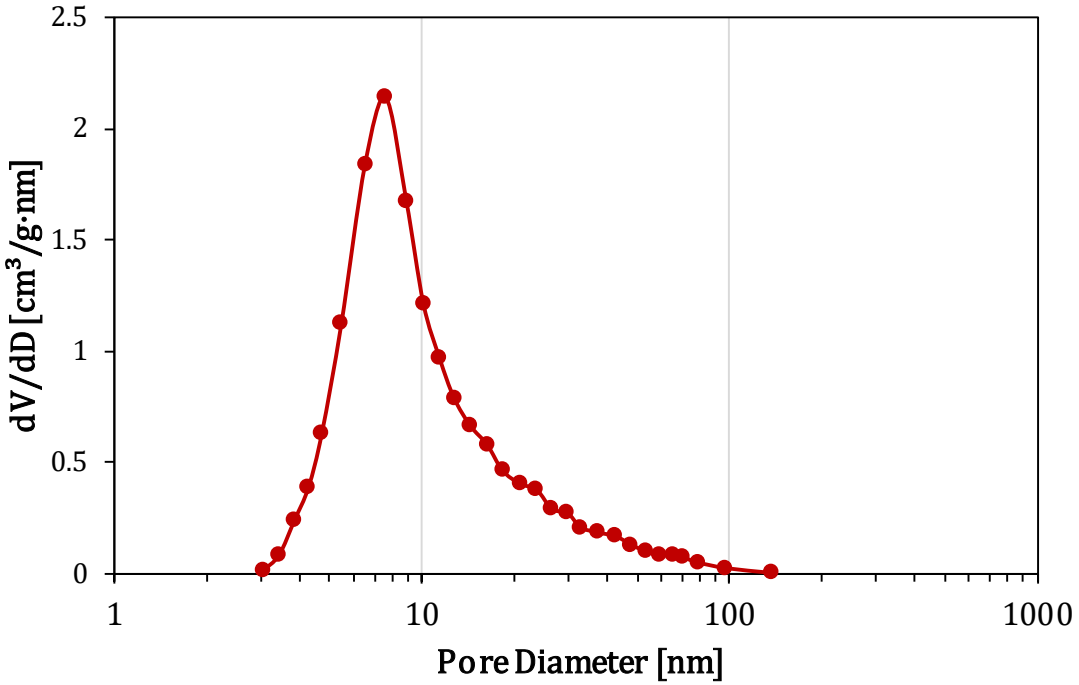

Figure S6 Pore size distribution of the SnO_2-NiO catalyst obtained from N_2 physisorption measurements.

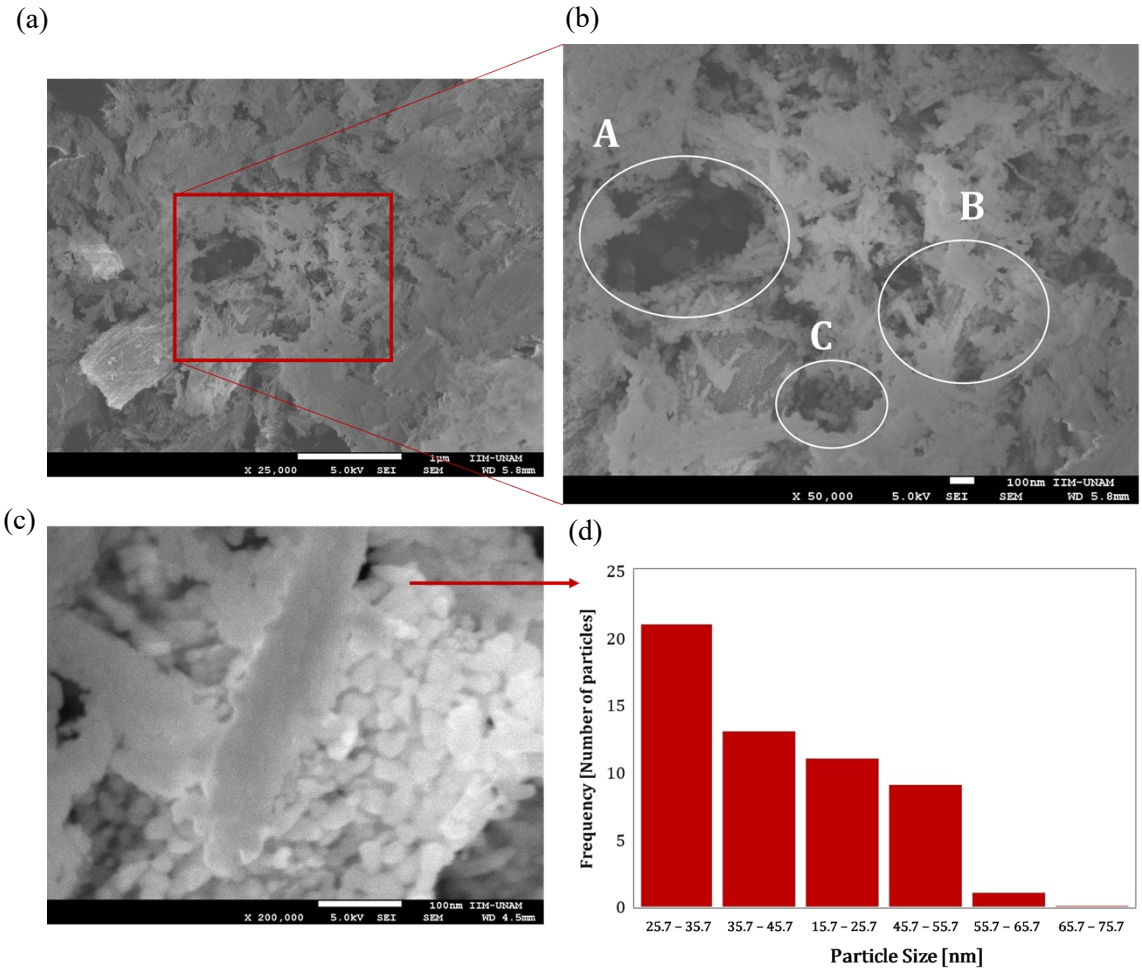

Figure S7 SEM images of SnO_2-NiO. d) – 1 μm; e) – 100 nm. The three circles are associated with: A - macroscopic structure; B - Slit-structured mesopores; C - Circular, flaky structure ; f) 100 nm; and g) particle size distribution.

Supplementary §5 Capability of the kinetic models for describing outlet molar flow rates.

This section presents the performance of the LHHW, ER and MvK models describing molar flows of species i at a wide range of operating conditions.

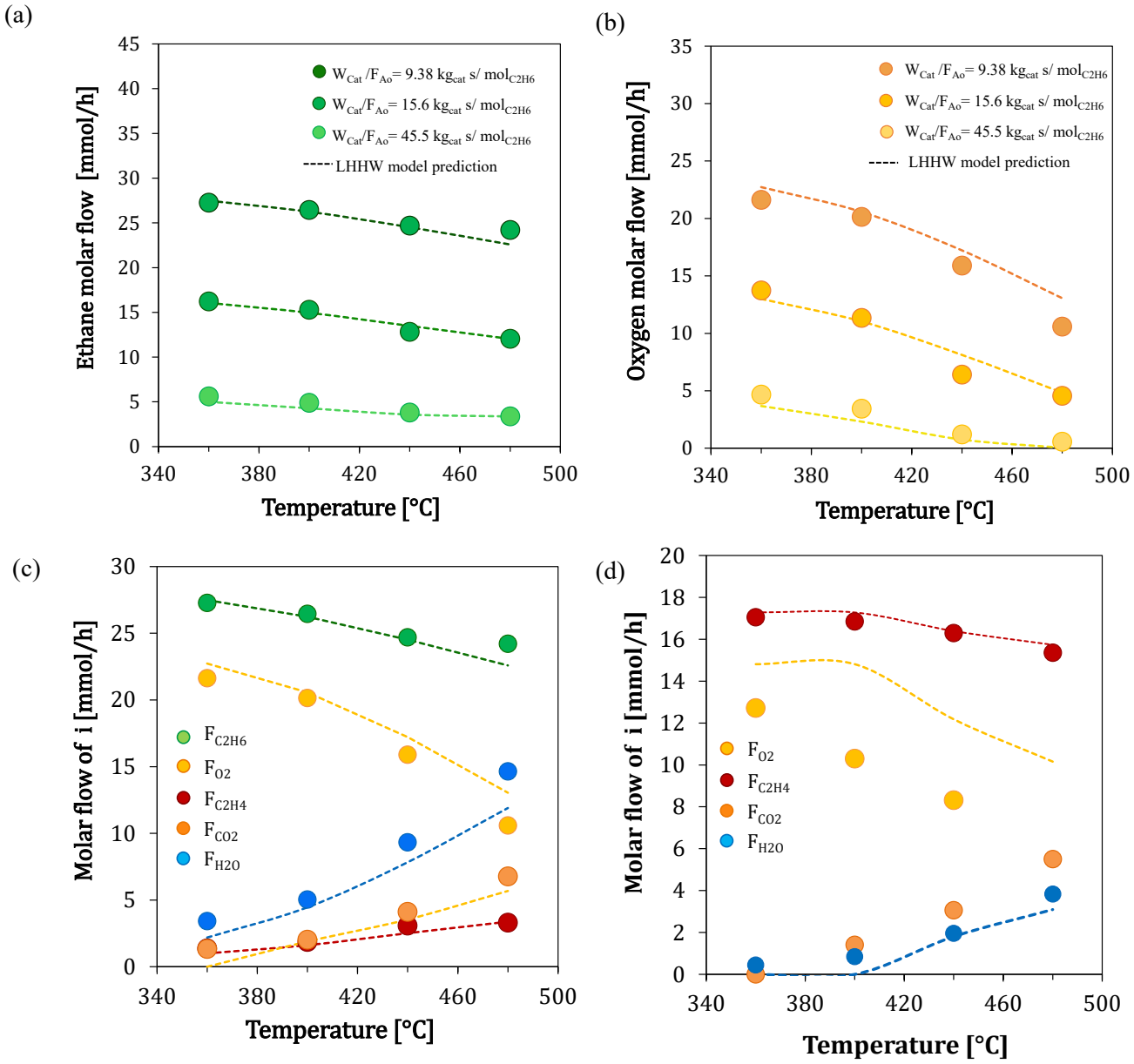

Figure S8. LHHW model performance. a) Ethane molar flow predictions, b) oxygen molar flow predictions, c) predictions of the molar flow of different species at different temperatures and at an space time of 9.38 kg_{cat} s/ mol_{C2H6} for the ODH of ethane and d) predictions of the molar flow of different species at different temperatures and at an space time of of 9.38 kg_{cat} s/ mol_{C2H6}) for the ODH of ethylene.

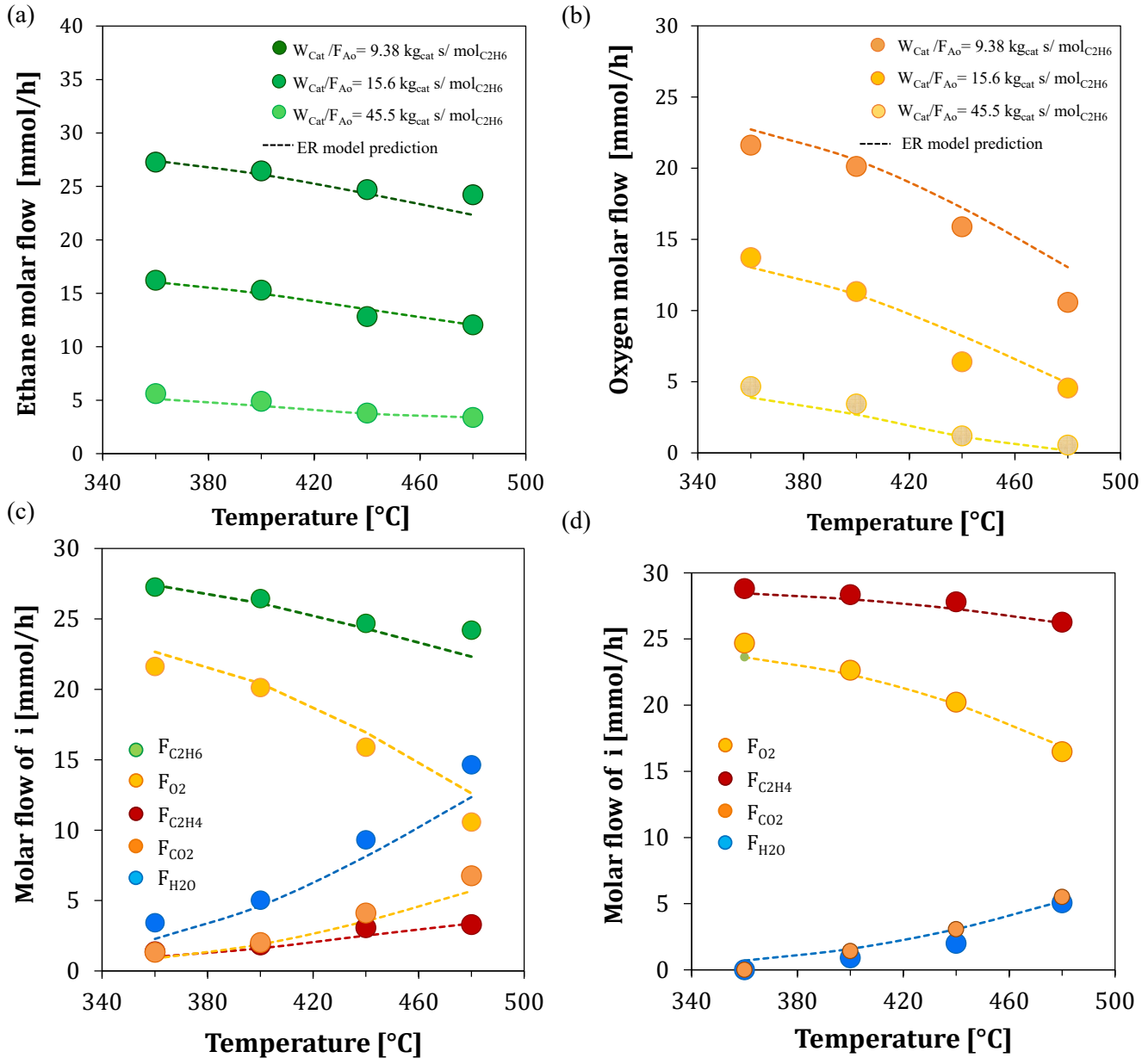

Figure S9. ER model performance. a) Ethane molar flow predictions, b) oxygen molar flow predictions, c) predictions of the molar flow of different species at different temperatures and at an space time of 9.38 kg_{cat} s/ mol_{C2H6} for the ODH feeding ethane and d) predictions of the molar flow of different species at different temperatures and at an space time of of 9.38 kg_{cat} s/ mol_{C2H6}) for the ODH feeding ethylene.

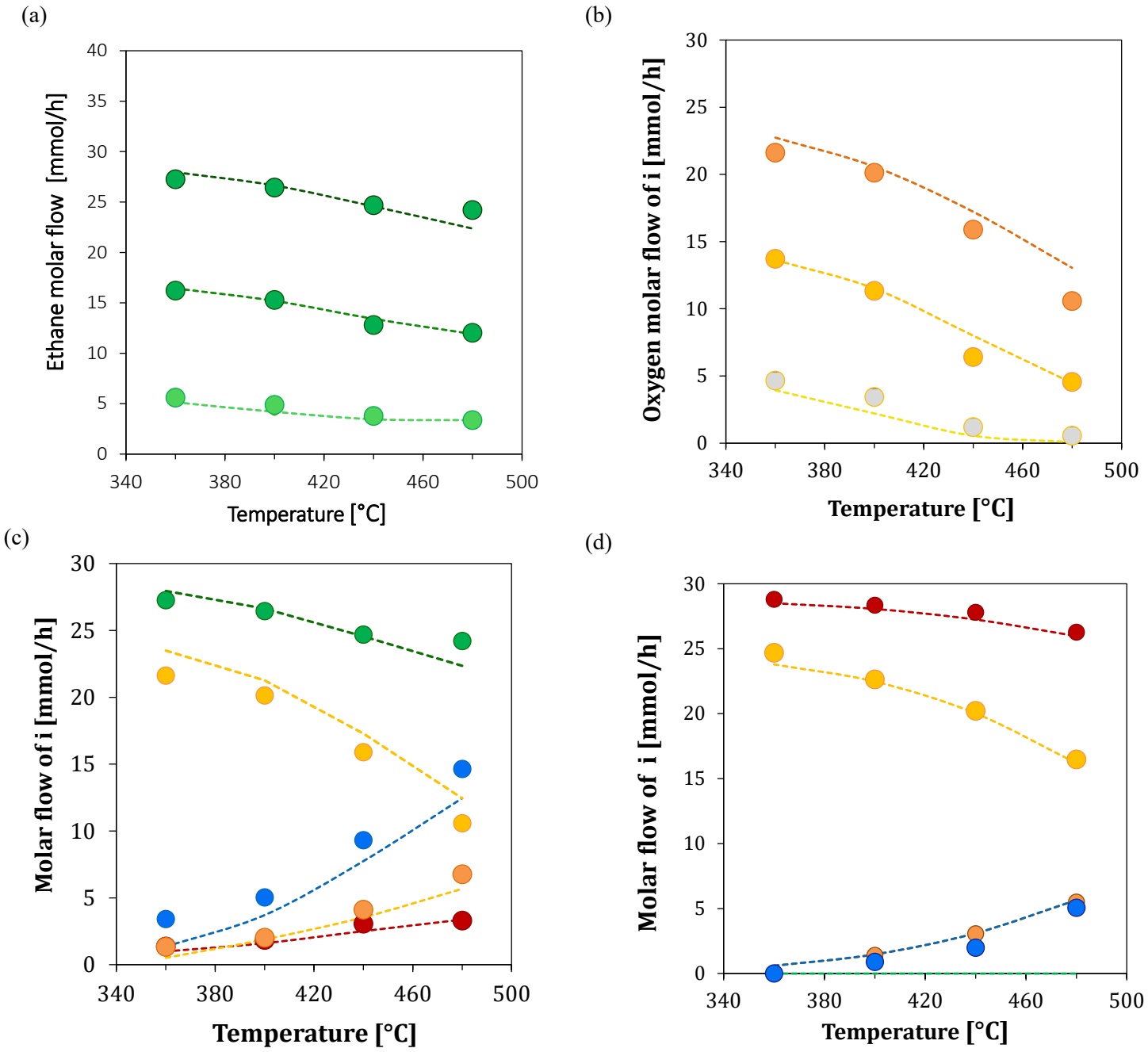

Figure S10. MvK model performance. a) Ethane molar flow predictions, b) oxygen molar flow predictions, c) predictions of the molar flow of different species at different temperatures and at an space time of 9.38 kg_{cat} s/ mol_{C2H6} for the ODH feeding ethane and d) predictions of the molar flow of different species at different temperatures and at an space time of of 9.38 kg_{cat} s/ mol_{C2H6}) for the ODH feeding ethylene.

Supplementary §6 Random residuals.

This section presents the residual of the responses. For all responses and operating conditions, the residuals are normally distributed around the x axis indicating no lack of fit by the model and a normal distribution of the experimental error.

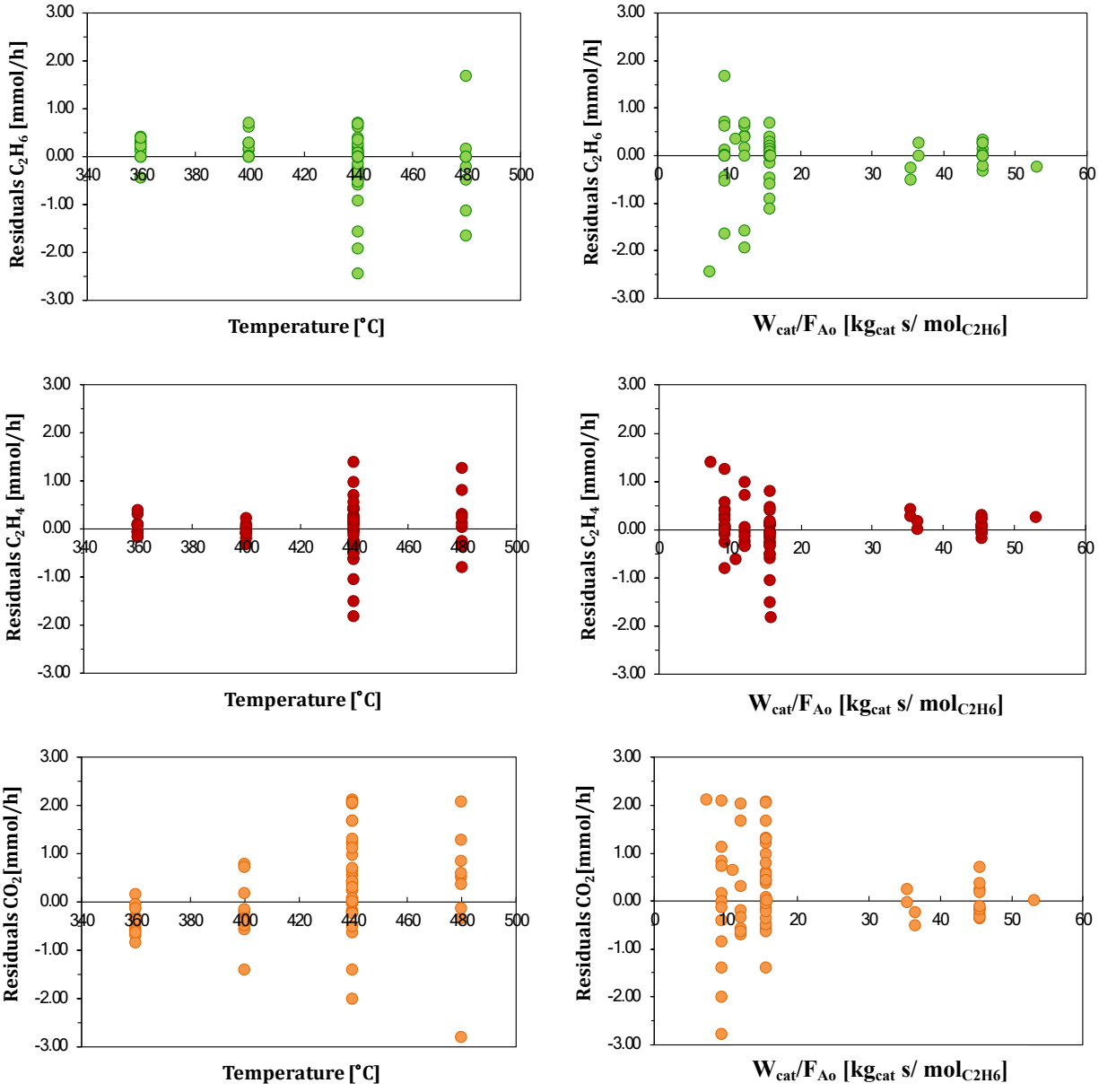

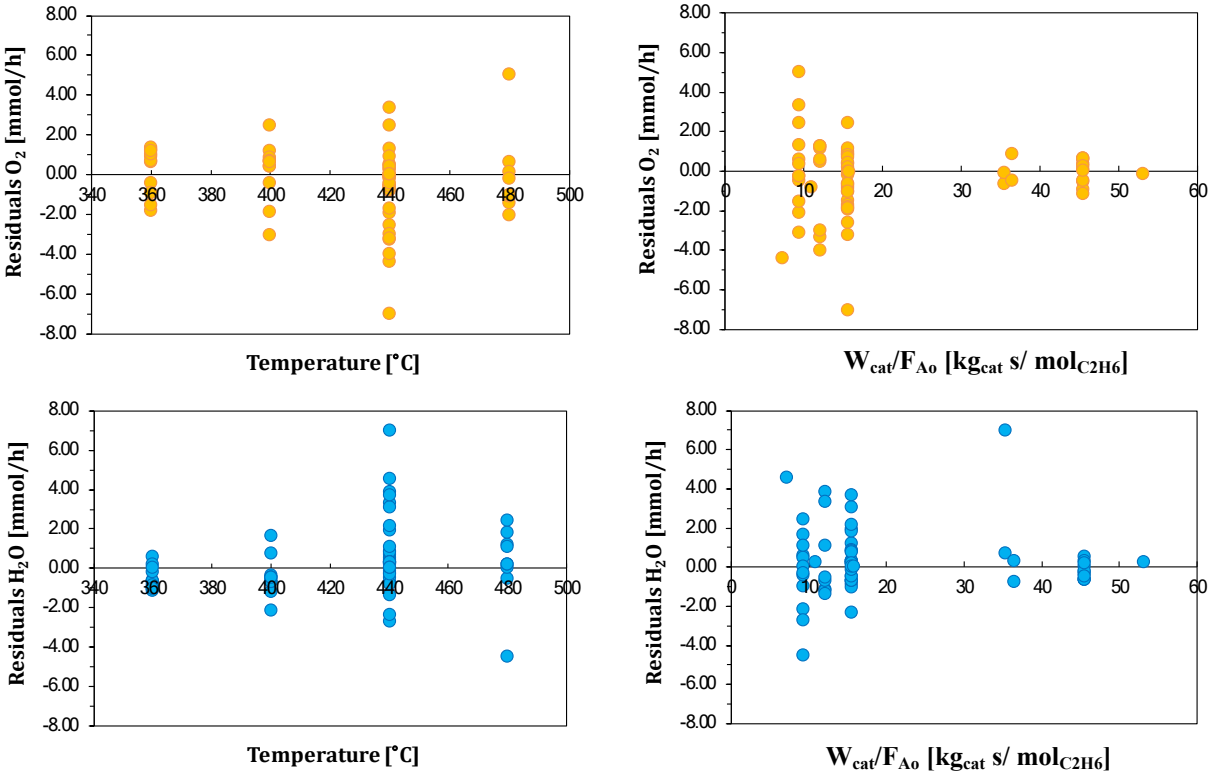

Figure S11. Residual figures for the molar outlet flow rate of C_2H_6, C_2H_4, CO_2, O_2 and H_2O as function of temperature (left) and space-time (right) obtained during the solution of the LHHW model under the pseudo-steady-state approach.

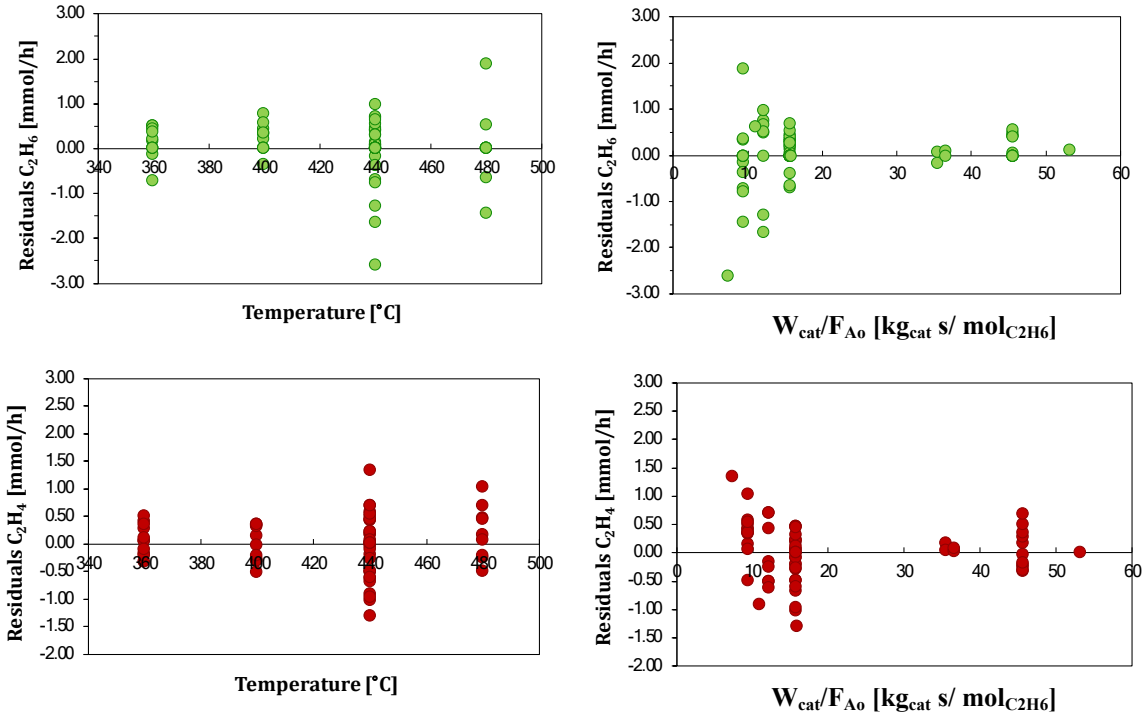

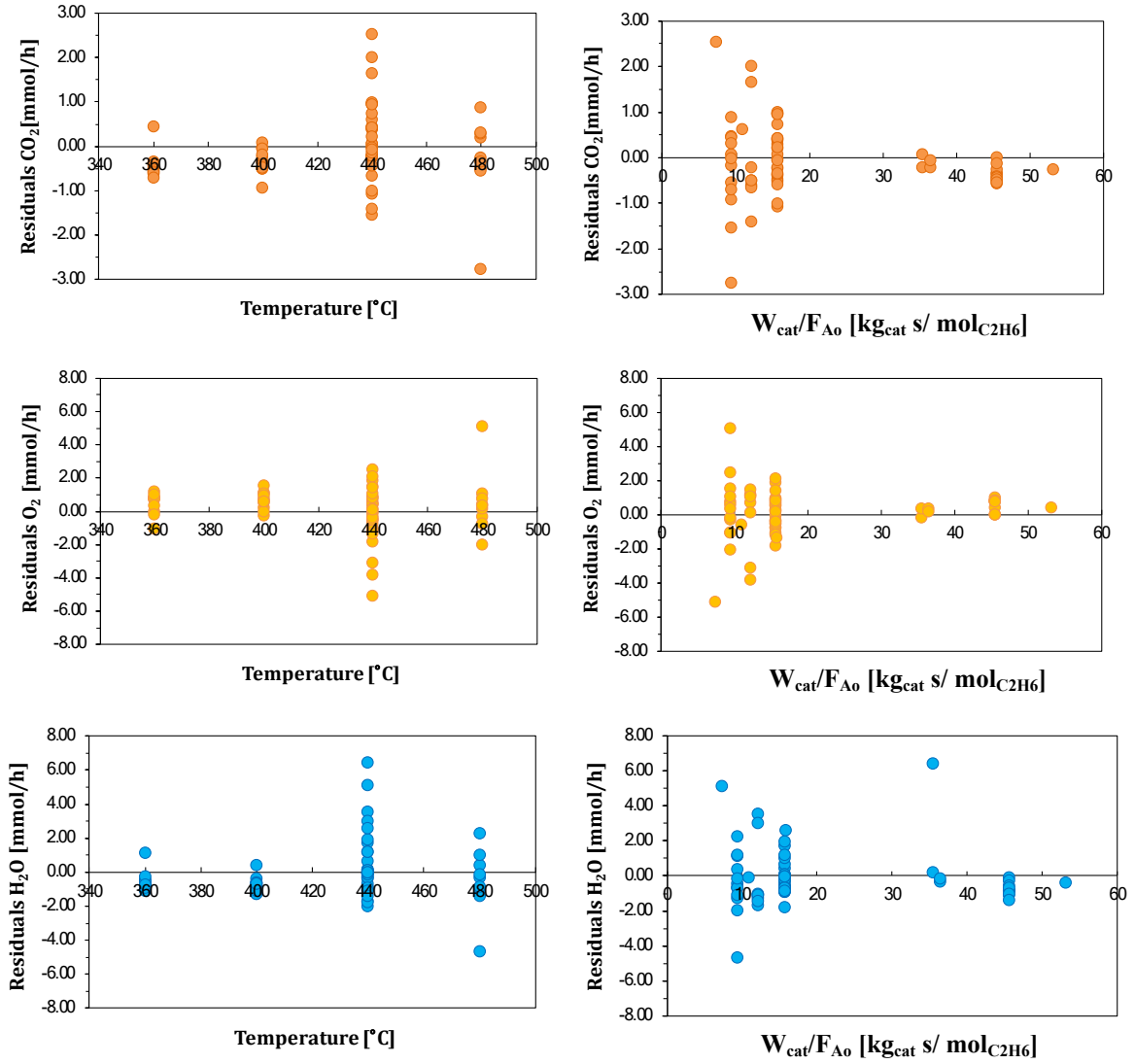

Figure S12. Residual figures for the molar outlet flow rate of C_2H_6, C_2H_4, CO_2, O_2 and H_2O as function of temperature (left) and space-time (right) obtained during the solution of the ER model under the pseudo-steady-state approach.

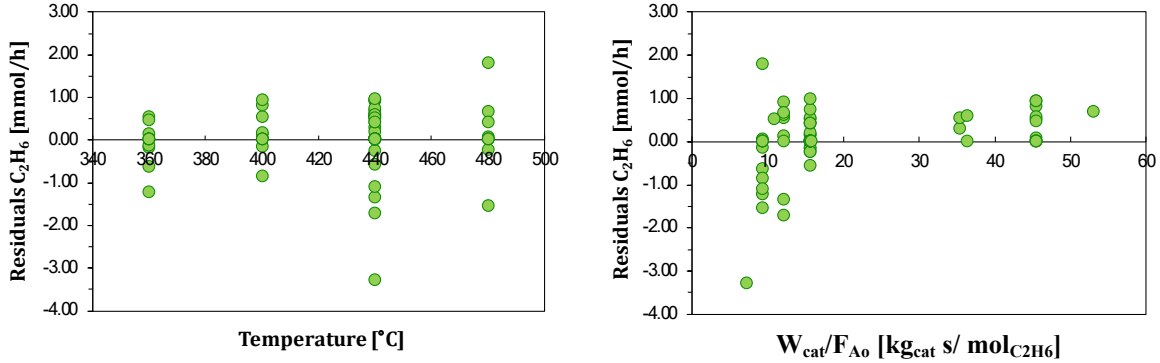

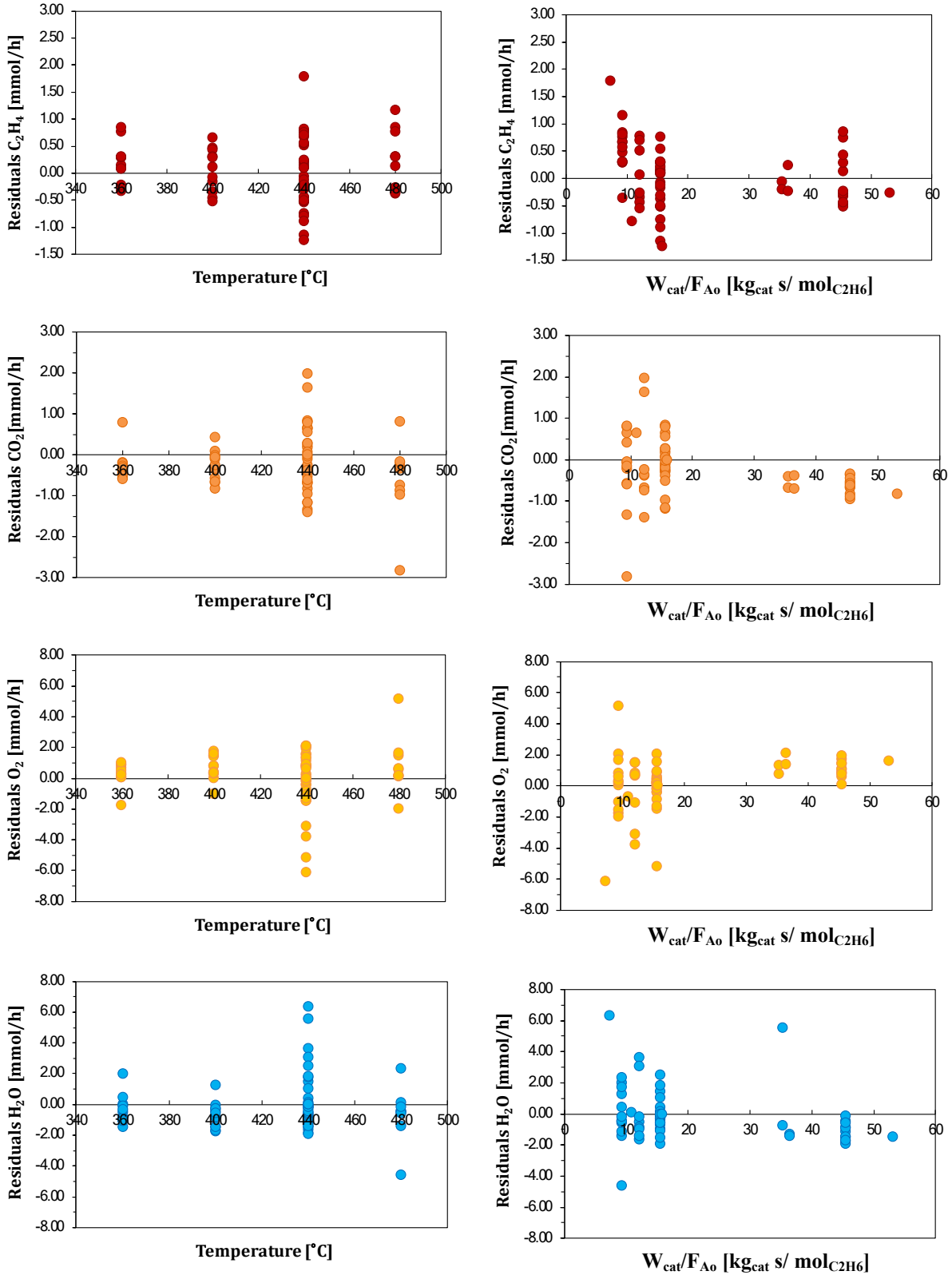

Figure S13. Residual figures for the molar outlet flow rate of C_2H_6, C_2H_4, CO_2, O_2 and H_2O as

function of temperature (left) and space-time (right) obtained during the solution of the MvK model under the pseudo-steady-state approach .

Supplementary §7 Binary correlation coefficient matrix.

This section presents the binary correlation coefficient matrix that gives information on the correlation strength between parameter pairs of parameters involved in the LHHW, ER and MvK models.

Table S2 . Binary correlation coefficient matrix as determined by non-isothermal regression to the experimental data for the LHHW model.

	Ea_1	Ea_2	Ea_3	Ea_{O2}^f	Ea_{O2}^r	Ea_{C2H6}^f	Ea_{C2H6}^r	Ea_{C2H4}^r	Ea_{C2H4}^f	Ea_{CO2}^r	Ea_{CO2}^f	Ea_{H2O}^r	Ea_{H2O}^f
Ea_1	1	-0.09	0.24	0.68	0.19	-0.4	0.08	0.45	0.17	-0.46	0.28	-0.7	0.07
Ea_2	-0.09	1	0.72	0.16	0.48	0.16	0.33	0.47	0.47	-0.19	0.33	-0.49	0.27
Ea_3	0.24	0.72	1	0.46	0.45	0.16	0.16	0.71	0.28	-0.4	0.48	-0.52	0.16
Ea_{O2}^f	0.68	0.16	0.46	1	0.07	-0.49	-0.28	0.59	-0.23	-0.61	0.4	-0.5	-0.29
Ea_{O2}^r	0.19	0.48	0.45	0.07	1	0.17	0.07	0.16	0.69	0.03	0.2	-0.61	0.03
Ea_{C2H6}^f	-0.4	0.16	0.16	-0.49	0.17	1	-0.03	-0.07	0.16	0.2	0.14	0.15	0.01
Ea_{C2H6}^r	0.08	0.33	0.16	-0.28	0.07	-0.03	1	0.1	0.44	0.06	-0.05	-0.12	0.81
Ea_{C2H4}^r	0.45	0.47	0.71	0.59	0.16	-0.07	0.1	1	0.16	-0.89	0.82	-0.54	0.16
Ea_{C2H4}^f	0.17	0.47	0.28	-0.23	0.69	0.16	0.44	0.16	1	0.08	0.09	-0.65	0.51
Ea_{CO2}^r	-0.46	-0.19	-0.4	-0.61	0.03	0.2	0.06	-0.89	0.08	1	-0.85	0.38	0.01
Ea_{CO2}^f	0.28	0.33	0.48	0.4	0.2	0.14	-0.05	0.82	0.09	-0.85	1	-0.38	0
Ea_{H2O}^r	-0.7	-0.49	-0.52	-0.5	-0.61	0.15	-0.12	-0.54	-0.65	0.38	-0.38	1	-0.17
Ea_{H2O}^f	0.07	0.27	0.16	-0.29	0.03	0.01	0.81	0.16	0.51	0.01	0	-0.17	1

Table S3 . Binary correlation coefficient matrix as determined by non-isothermal regression to the experimental data for the ER model.

	Ea_1	Ea_2	Ea_3	Ea_{O2}^{f}	Ea_{O2}^{r}	Ea_{H2O}^{r}	Ea_{H2O}^{f}
Ea_1	1	0.05	0.01	-0.25	0.13	0.16	-0.91
Ea_2	0.05	1	0.21	-0.2	0.05	0.34	-0.07
Ea_3	0.01	0.21	1	0.25	0.03	-0.15	0.04
Ea_{O2}^{f}	-0.25	-0.2	0.25	1	-0.04	-0.02	0.33
Ea_{O2}^{r}	0.13	0.05	0.03	-0.04	1	0.01	-0.03
Ea_{H2O}^{r}	0.16	0.34	-0.15	-0.02	0.01	1	-0.22
Ea_{H2O}^{f}	-0.91	-0.07	0.04	0.33	-0.03	-0.22	1

Table S4 . Binary correlation coefficient matrix as determined by non-isothermal regression to the experimental data for the MvK model.

	Ea_1	Ea_2	Ea_3	Ea_{Ox}^{f}	Ea_{Ox}^{r}
Ea_1	1	-0.418	0.131	-0.017	-0.340
Ea_2	-0.418	1	0.063	-0.374	0.520
Ea_3	0.131	0.063	1	-0.211	0.139
Ea_{Ox}^{f}	-0.017	-0.374	-0.211	1	0.006
Ea_{Ox}^{r}	-0.340	0.520	0.139	0.006	1

BIC criterion

The model discrimination is performed based on the Bayesian Information Criterion (BIC). The model for which the lowest BIC value is calculated, using Eq. (29), is considered to be the statistically best performing model.

$$\mathrm{BIC} = N \ln\left(\frac{RSS}{N}\right) + p \ln(N) \qquad \text{* MERGEFORMAT (29)}$$

In Eq. (29) N is the number of observations, RSS is the residual sum of squares obtained during the adjustment of the data, and p is the number of parameters to estimate.